# SUPRAMOLECULAR ARCHITECTURE, CHARACTERIZATION AND COMPUTATIONAL STUDIES OF HYDRAZINIUM PICRATE – AN ORGANIC CHARGE TRANSFER CRYSTAL

S. Sivaraman[a], R. Markkandan [a]*, SP. Meenakshisundaram[a]
[a]Department of Chemistry, Annamalai University, Annamalainagar-608 002, Tamilnadu, India

**A B S T R A C T**

**Single crystals of hydrazinium picrate were grown by the slow evaporation solution growth technique from ethanol at room temperature. The crystals belong to the monoclinic system with centrosymmetric space group. The crystallinity of the material was confirmed by powder X-ray diffraction analysis. The functional groups present in the molecule are identified by FT-IR analysis and the band gap energy is estimated using diffuse reflectance data by the application of Kubelka–Munk algorithm. The thermal stability of the compound was investigated by carrying out TG-DTA analysis. Photoluminescence studies were also carried out for the grown crystal. The molecules are associated by weak C-H…O, N-H…O and π-π stacking interactions, which are responsible for the formation and strengthening of the supramolecular assembly. Inter- and intramolecular hydrogen-bonding interactions support the supramolecular architecture in the crystal packing. Theoretical calculations were performed using density functional theory (DFT) to derive the optimized geometry, dipole moment, HOMO–LUMO energies and first-order molecular hyperpolarizability(β). The intermolecular hydrogen bonding interactions are analyzed by Hirshfeld surface analysis and fingerprint plots.**

**Keywords: Supramolecular architecture, Charge transfer, Hirshfeld analysis, Hyperpolarizability**

## 1. Introduction

Picric acid as an electron acceptor form charge transfer molecular complexes with a number of electron donor compounds such as amines through electrostatic or hydrogen bonding interactions and he bonding depends on the nature of the donor–acceptor. Recently, numbers of hydrazide complexes possessing high macro level nonlinearity are reported [1-3]. The organic nonlinear optical (NLO) materials have excellent NLO susceptibilities and electro-optical susceptibilities [4]. The organic crystals having higher hyperpolarizabilities, lower dielectric constant and thermal stabilities are expected to have high NLO properties. A conjugated structure is possible to those crystals having charge transfer between electron acceptors and donors [5-8]. Molecular structure of 4-Nitrophenylhydrazinium picrate monohydrate [9] and 1-Methylhydrazinium picrate [10] have been reported. In present article, we demonstrate the synthesis, supramolecular architecture, thermal, optical, photoluminescence, Hirshfeld surface analysis and first order hyperpolarizability studies of title crystal. Observed NLO response is rationalized.

## 2. Experimental

### *2.1 Synthesis*

FHM was synthesized by mixing stoichiometric quantities of picric acid and 2-furic hydrazide in the molar ratio of 1:1. The mixture was stirred at room temperature for 3 h and it was obtained as a yellow precipitate. The product was purified by recrystallization using an ethanol solvent system. Transparent crystals were grown by the slow evaporation solution growth technique and the crystals were harvested after a period of 5–10 d. Crystal image, morphology and SEM image of FHM are shown in Fig.1.

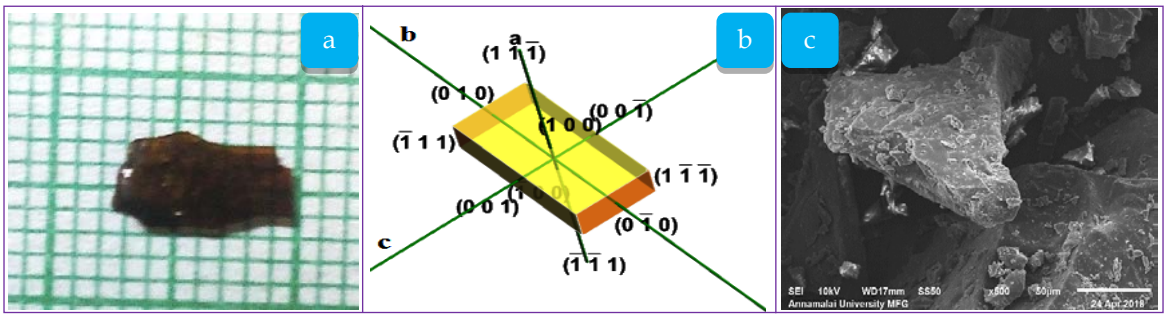


**Fig.1 (**a) Photo image (b) Crystal morphology (c) SEM image

## 2.2 Characterization techniques

The structural analysis was carried out for a selected sample of approximately 0.150 × 0.100 × 0.100 mm3 size using BRUKER AXS (Kappa APEXII) X-ray diffract meter employing graphite monochromated Mo Kα radiation (λ = 0.71073Å). FT-IR spectra were recorded using an AVATAR 330 FT-IR by KBr pellet technique in the spectral range of 600-4000 cm-1. Morphologies of the samples are observed on a JEOL JSM 5610 LV scanning electron microscope with the resolution of 12 mm, an accelerating voltage of 15 kV and maximum magnification 500 x and 2000 x. Bulk samples were analyzed by PXRD with a Bruker D8 powder diffractometer (BrukerAXS, Karlsruhe, Germany). Experimental conditions: Cu Kα radiation (λ=1.54056 A˚); 40 kV; 30 mA; scanning interval 10-90o, 2θ at a scan rate of $1^{o}$ $min^{-1}$; time per step 0.5s. Diffuse reflectance spectra of the samples were recorded using the DRA-CA-30I accessory and converted to absorption spectra using the Kubelka-Munk function. The UV-DRS spectrum was measured in the region of 200–700 nm. Photoluminescence of the sample were analyzed by FLUOROLOG-FL3-11 accessory.

## 2.3Computational details

Computational studies were done using the GAUSSIAN09W [11] software package without any constraints on the geometry using density functional theory (DFT) and the molecules were visualized with the GAUSSVIEW 5.0 program [12]. Hirshfeld surfaces, electrostatic potential and fingerprint plots were generated by from the crystal data using the DFT method with 6-31G(d, p) as the basis set [13] and deformation density is generated from Crystal Explorer (Version 3.1), using DFT method with 6-31G(d,p) as basis set [14]. The WinXMorph software 3.5 was used to infer the morphology of the FHM crystal with the help of crystallographic Information File (CIF) from a grown crystal as an input [15]. Simulated powder XRD pattern and crystal packing were visualized by mercury 3.5.1 software [16].

## 3. Results and discussion

### *3.1 FT-IR spectroscopy*

Vibrational IR spectrum of FHM is shown in Fig.2. The band at 1614 $cm^{-1}$ is due to N-H stretching frequency. The phenolic O vibration is observed at 1158 $cm^{-1}$. The $NH(NH_3^+)$ symmetric stretching vibration appeared as a sharp intensity band around 3098 $cm^{-1}$. The absorption band around 3593 $cm^{-1}$ corresponds to O-H stretching vibrations. The $NO_2$ stretching vibration appeared as sharp intensity band around 1333 $cm^{-1}$

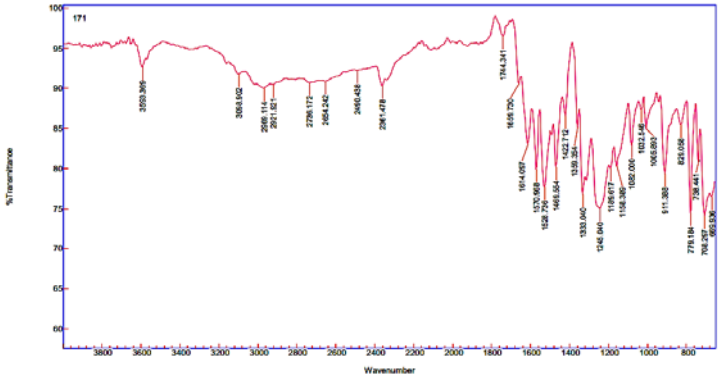


**Fig.2** FT-IR spectrum of FHM

### *3.2 XRD*

The as-grown FPMI crystal was finely powdered and subjected to powder XRD analysis. The indexed powder XRD pattern of the as-grown FPMI is shown in Fig.3 along with the simulated one. The XRD profiles show that the sample is of single phase without a detectable impurity. The well defined Bragg peaks at specific 2θ angles show the high crystallinity of the material. Most of the peak positions in the powder and simulated X-ray diffraction patterns from the single crystal XRD analysis coincide but the relative intensities differ. Possibly this could be due to the preferred orientation of the sample used for the diffractogram measurement. Also, the difference mosaic spread of the powder and single crystal patterns contribute to intensity variations.

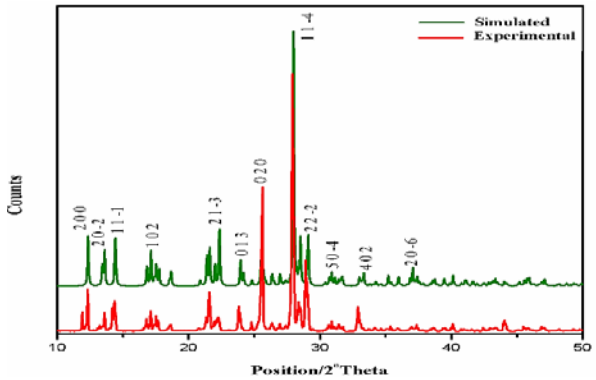


**Fig.3** Powder XRD Pattern

### *3.3 Single crystal XRD*

Single crystals of 2-furic hydrazinium picrate monohydrate (FHM) belongs to monoclinic system with centrosymmetric space group P21/c and the unit cell parameters are, a = 16.0147(18) Å, b = 6.9540(8) Å c = 14.7166(16) Å V = 1467.2(3) Å3 and Z = 4. Crystal data is listed in Table 1. The structure is determined with a low value of R factor (0.1153) using 14329 reflections (R(int) = (0.0487) and goodness of fit, (F2) = 1.015. An ORTEP view and packing diagram of FHM are shown in Fig.4. The structure comprises 2-furic hydrazinium cations and one picrate anions coordinate to the one water molecule. The donor and acceptor molecules of complex are held together by van der Waals interactions. The bond lengths of C(1)–C(2) and C(1)–C(6)° are 1.449(4) and 1.450(4) Å respectively which are longer and deviate from regular aromatic C-C values. The C(1)-O(7) bond distance in FHM is 1.255(3) Å, which is intermediate between the single and double bonds. Loss of hydroxyl proton at the O(7) leading to specific electron delocalization around C(1) is observed. These observations are in agreement with the other picrates subjected to proton transfer. It has been established that the orientation of anion and cation facilitates the formation of N–H…O hydrogen bonds between hydrazine nitrogen and phenolic oxygen. The crystal structure is stabilized by hydrogen bonds and specific short contacts. Table 2 lists the hydrogen bonds and symmetry transformations. The strong hydrogen bonds like O–H…O and N–H…O contribute to charge transfer, hence nonlinearity and resulting in nonlinear optical character. Weak intermolecular interactions are observed for N(5)-H(5A)...O(6), N(5)-H(5A)...O(9) and C(9)-H(9)...O(1) with bond distances of 2.66(3), 2.64(3) and 2.63Å.

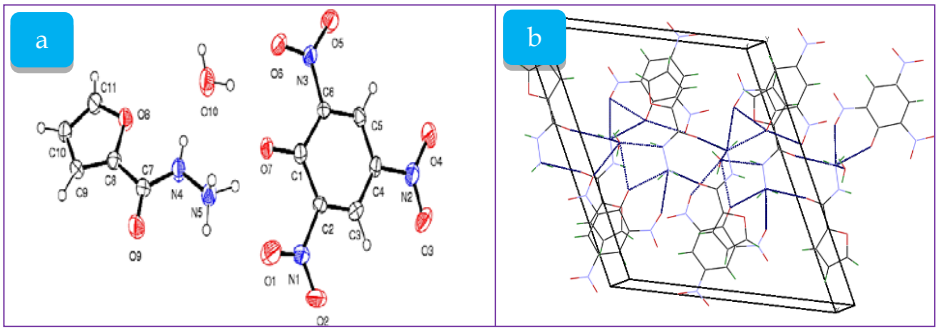


**Fig.4** a) ORTEP of FHM b) Molecular packing in the unit cell

The supramolecular architecture of the hydrogen- and ionically bonded network structure is clearly shown by X-ray analysis. The geometry of the 2-furic hydrazinium picrate monohydrate was found to be governed by π - π, C-H…O and N-H…O hydrogen bonds, with water molecules interconnecting the molecules. The π – π interactions exhibited by FHM are displayed in Fig.S1. In FHM, the furan rings and picrate C-C in inter-columnar spaces are connected together by edge-to-edge π – π interactions with almost parallel planes. Fig.S2 shows the strong N-H…O interactions. The C-H…O interactions for FHM are displayed as Fig.S3. Crystal three-dimensional packing showing the inter- and intramolecular interactions along 'a', 'b' and 'c' axis are displayed in Figs.S4-S6. The packing looks like layers arranged as a ladder like chains along 'c' axis as shown in Fig. S6. The π…π interactions are seen with a distance of about 3.435 Å whereas the distances of π…π planes range from 3.435 to 3.816 Å. Crystal structure of FHM exhibits both inter and intra-molecular hydrogen-bonding interactions with different supramolecular infrastructures.

**Table 1** Crystal data and structure refinement for FHM

| **Empirical formula** | **$C_{11}$ $H_{11}$ $N_5$ $O_{10}$** |
|---|---|
| Formula weight | 373.25 |
| Temperature | 296(2) K |
| Wavelength | 0.71073 Å |
| Crystal system | Monoclinic |
| Space group | $P2_1/c$ |
| Unit cell dimensions | a = 16.0147(18) Å α= 90°<br>b = 6.9540(8) Å β= 116.460(3)°<br>c = 14.7166(16) Å γ = 90° |
| Volume | 1467.2(3) $Å^3$ |
| Z | 4 |
| Density (calculated) | 1.690 $Mg/m^3$ |
| Absorption coefficient | 0.152 $mm^{-1}$ |
| F(000) | 768 |
| Crystal size | 0.150 x 0.100 x 0.100 $mm^3$ |
| Theta range for data collection | 2.768 to 25.473°. |
| Index ranges | -19<=h<=19, -8<=k<=8, -17<=l<=17 |
| Reflections collected | 14329 |
| Independent reflections | 2727 [R(int) = 0.0719] |
| Completeness to theta | = 25.242° , 100.0 % |
| Absorption correction | Semi-empirical from equivalents |
| Max. and min. transmission | 0.7453 and 0.6743 |
| Refinement method | Full-matrix least-squares on $F^2$ |
| Data / restraints / parameters | 2727 / 10 / 259 |
| Goodness-of-fit on $F^2$ | 1.015 |
| Final R indices [I>2sigma(I)] | R1 = 0.0487, wR2 = 0.1038 |
| R indices (all data) | R1 = 0.1153, wR2 = 0.1292 |
| Largest diff. peak and hole | 0.346 and -0.353 $e.Å^{-3}$ |

**Table 2** Hydrogen bonds for FHM [Å and °].

| D-H...A | d(D-H) | d(H...A) | d(D...A) | <(DHA) |
|---|---|---|---|---|
| C(9)-H(9)...O(1)#1 | 0.93 | 2.63 | 3.460(4) | 148.7 |
| C(10)-H(10)...O(4)#2 | 0.93 | 2.56 | 3.174(4) | 123.7 |
| C(11)-H(11)...O(3)#3 | 0.93 | 2.37 | 3.165(4) | 143.9 |
| C(11)-H(11)...O(5)#4 | 0.93 | 2.55 | 3.127(4) | 120.7 |
| O(10)-H(10A)...O(6) | 0.847(18) | 2.05(3) | 2.768(3) | 142(3) |
| O(10)-H(10A)...O(7) | 0.847(18) | 2.09(3) | 2.767(3) | 137(3) |
| O(10)-H(10B)...O(9)#5 | 0.851(19) | 2.64(3) | 3.422(4) | 153(3) |
| N(5)-H(5A)...O(6)#6 | 0.853(17) | 2.66(3) | 3.072(4) | 111(2) |
| N(5)-H(5A)...O(9)#1 | 0.853(17) | 2.217(18) | 3.031(4) | 160(3) |
| N(5)-H(5B)...O(1) | 0.885(16) | 2.17(3) | 2.759(4) | 123(3) |
| N(5)-H(5B)...O(7) | 0.885(16) | 1.959(18) | 2.797(3) | 158(3) |
| N(4)-H(4A)...O(10) | 0.838(18) | 1.96(2) | 2.770(4) | 163(3) |
| N(5)-H(5C)...O(5)#6 | 0.863(16) | 2.58(3) | 3.079(4) | 118(3) |
| N(5)-H(5C)...O(10)#7 | 0.863(16) | 2.071(18) | 2.890(5) | 158(3) |

Symmetry transformations used to generate equivalent atoms:
#1 -x+1,-y+1,-z #2 x-1,y,z-1 #3 x-1,-y+3/2,z-1/2 #4 -x+1,-y+1,-z+1 #5 x,-y+1/2,z+1/2 #6 x,-y+1/2,z-1/2 #7 -x+1,y-1/2,-z+1/2

### *3.4 Thermal analysis*

The grown FHM crystal has been crushed into fine powder, and the powder form of the weighted (33.63 mg) sample is added into Al2O3 crucible and heated from room temperature (RT) to 600 ºC at a heating rate of 20 ºC/min in an inert nitrogen atmosphere. Fig.5 shows the TG-DTA profile of FHM. In the TG trace, FHM was stable up to 117° C. The major weight loss of 69.9 % occurred between 117 °C and 417 °C which was due to the decomposition and volatilization of the compound. The final residue left at 592°C is 21.60%. In DTA curve, the first endothermic peak appears at 132°C corresponding to the melting point of FHM crystal and which merely coincides with the TG curve.

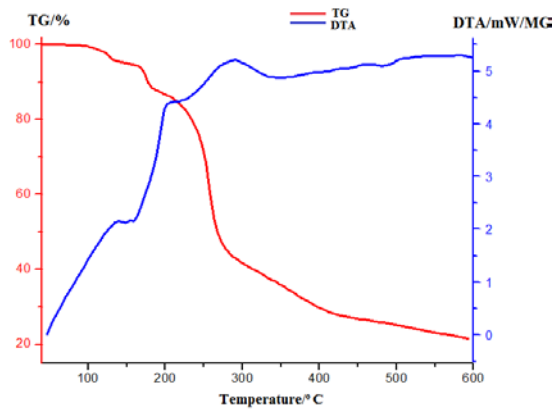


**Fig.5** TG-DTA curve

### *3.5 UV-Vis-NIR diffuse reflectance spectrum*

The optical absorption spectrum shows the absorption is minimum in the visible region and cut-off wavelength is ~509 nm. The Kubelka–Munk theory provides a correlation between reflectance and concentration. The direct band gap energy of the specimen is estimated as 2.44 eV from the Tauc plot [F(R)hv]2 versus hv(eV)(Fig.6).

$$F(R)=(1-R)2/2R= \alpha/s = Ac/s$$

where F(R) is the Kubelka–Munk function, R is the reflectance of the crystal, α is the absorption coefficient and S is the scattering coefficient, A is the absorbance and c is the concentration of the absorbing species. The wide transparency ranges from visible to near infrared.

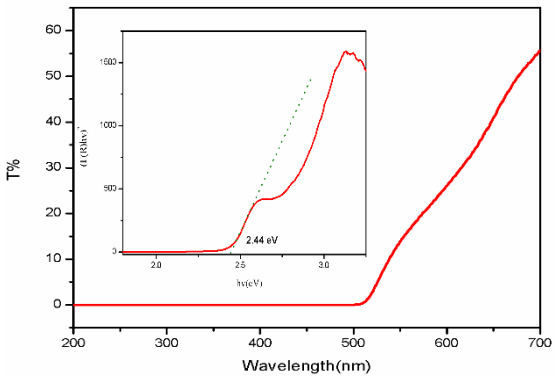


**Fig.6** UV- vis spectrum (Tauc plot is given as an inset) of FHM

### *3.6 Photoluminescence studies*

The photoluminescence (PL) study affords information on the emission characteristics of the materials at the molecular level, which include deep and shallow level deformities and energy vacuum states [16]. The luminescence characteristic of the grown crystal is analyzed by exciting it at 509 nm. Fig.7 displays the

emission spectrum of the FHM crystal recorded at room temperature. A broad green emission peak was observed at 529 nm, attributed to the π-π* of the picrate chromospheres in the FHM crystal. The luminescent nature recommends that the FHM crystal with the high emission intensity can be used as green light emitter and for optical device applications [17].

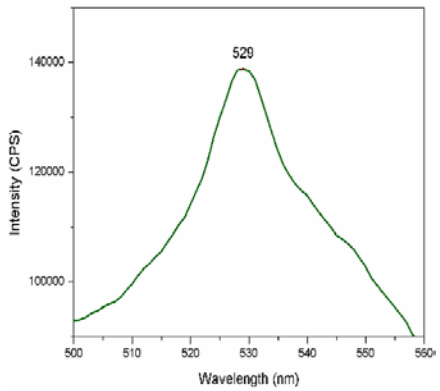


**Fig. 7** Photoluminescence spectrum of FHM crystal

### *3.7 First-order molecular hyperpolarizability*

The calculated first-order molecular hyperpolarizability (β) and dipole moment (μ) of the specimen are 9.7703 × 10− 30 esu (37 times that of urea) and 13.4824 D, respectively. The high hyperpolarizability is due to the nonzero β values. High (β) value is associated with high charge transfer. It is strong inter- and intramolecular hydrogen bonding enhance the hyperpolarizability leading to nonlinearity. It is clear from Table 3 that the delocalization of electron cloud is more along x direction because of its large contribution to β total value.

**Table 3** First-order molecular hyperpolarizability(β) and dipole moment (μ) of FHM

| **First-order molecular hyperpolarizability** | |
|---|---|
| $\beta_{xxx}$ | 1370.642 |
| $\beta_{xxy}$ | -418.773 |
| $\beta_{xyy}$ | -434.890 |
| $\beta_{yyy}$ | -31.537 |
| $\beta_{xxz}$ | -57.925 |
| $\beta_{xyz}$ | -149.809 |
| $\beta_{yyz}$ | 152.135 |
| $\beta_{xzz}$ | 79.453 |
| $\beta_{yzz}$ | -26.547 |
| $\beta_{zzz}$ | 50.596 |
| $\beta_{tot}$( X $10^{-30}$)esu | 9.770 |
| **Dipole moment** | |
| $\mu_x$ | -5.1679 |
| $\mu_y$ | 1.8733 |
| $\mu_z$ | 1.1945 |
| μ | 13.824 |

### *3.8 Frontier molecular orbitals*

Frontier molecular orbital's FMOs are the highest occupied molecular orbital (HOMO) and the lowest unoccupied molecular orbital (LUMO). These FMOs play a major role in the study of electrical, optical and chemical properties of the compounds. The HOMO shows various prominent donor orbitals and the LUMO shows that of prominent acceptor orbitals. The electronic absorption is due to the transition from the ground state to the first excited state i.e., an electron is excited from the highest occupied molecular orbital (HOMO) to the lowest unoccupied molecular orbital (LUMO). The obtained FMOs are shown in Fig.8. The obtained HOMO value is – 6.62 eV while LUMO value is – 2.72 eV, and the ΔE

value calculated at the DFT level is 3.89 eV. The theoretical energy band gap value obtained from FMOs is somewhat higher than the experimental value. This can be well attributed towards the alienated FHM molecule is in the gas phase whereas the obtained experimental value is in the solid phase [18].

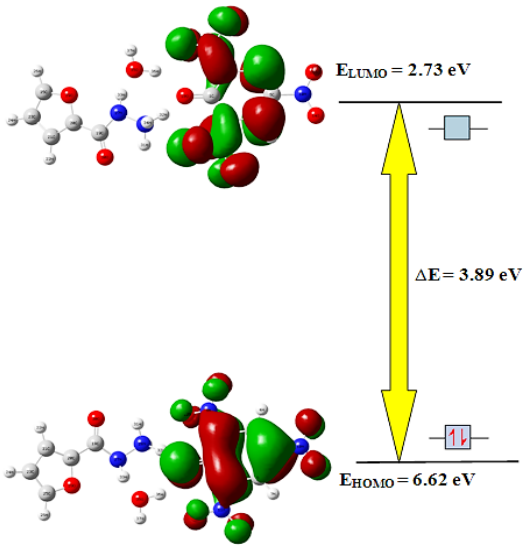


**Fig.8** Surfaces of Frontier Molecular Orbitals

### *3.9 Hirshfeld surfaces analysis*

The Hirshfeld surfaces [19-21] of FHM are displayed in Fig. 9, showing surfaces that have been mapped over a dnorm, shapeindex, curvedness, de (distance from the point to the nearest nucleus external to the surface) and di (distance to the nearest nucleus internal to the surface). The normalized contact distance (dnorm) based on both de and di. Shapeindex provides π-π interaction information. The curvedness surface indicates the electron density surface curves around the molecular interactions. The surfaces are shown as transparent to allow visualization of the FHM molecule around which they were calculated. The surface representing the circular depressions (deep red) visible on the Hirshfeld surface are indicative of hydrogen bonding contacts and other visible spots are due to O···H & H···O (53.4%), N···H & H···N (2.4%) C···H & H···C (6.9%), H···H (9.9%) and C-C (7.6%)(π-π) interactions as shown in Fig.10. The small range of area and light color on the surface represents a weaker and longer contact other than hydrogen bonds. The two-dimensional fingerprint plots of FHM clearly illustrate the intermolecular interactions pattern.

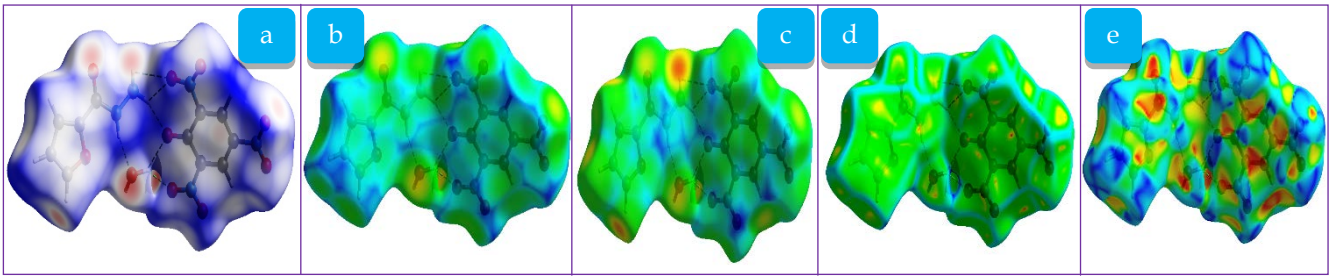


**Fig.9** Hirshfeld surfaces (a) The $d_{norm}$ (b) $d_i$, (c) $d_e$, (d) curvedness (e) shape index

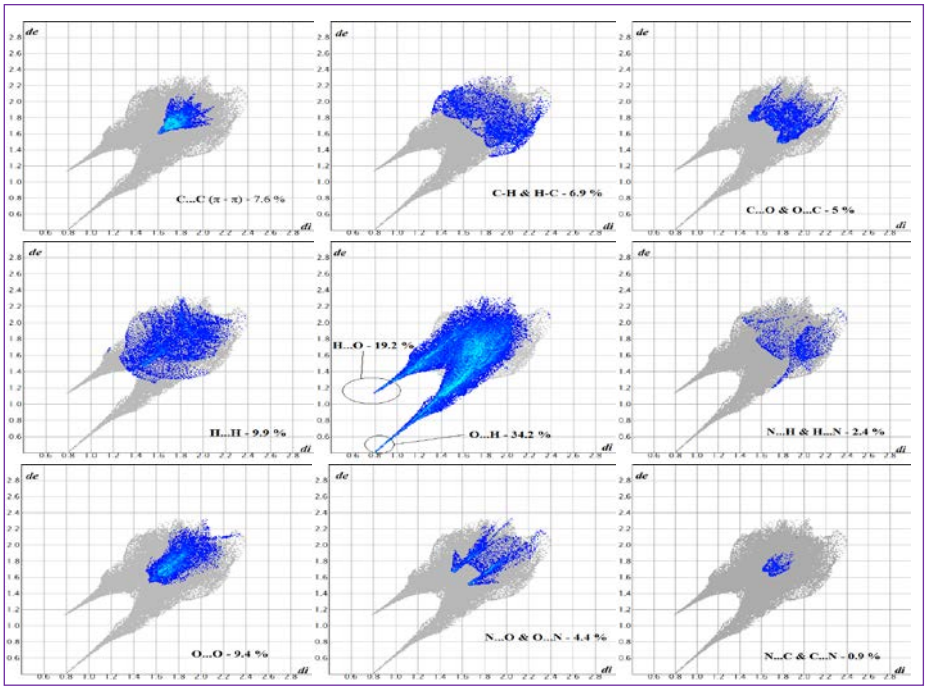


**Fig.10** 2D fingerprint plot interactions

## 4. Conclusions

Single crystals of 2-furic hydrazinium picrate monohydrate (FHM) were successfully grown as single crystals by the slow evaporation technique. It crystallizes in the centric monoclinic system with P21/c as a space group. The FT-IR analysis confirms the presence of functional groups constituting FHM. Band gap energy estimated. The TG-DTA studies elucidated the decomposition and confirmed the thermal stability and suggested that it could be used in optical applications below its melting point (117°C). The analysis of Hirshfeld surface derived fingerprint plots is an effective method to identify the different types of intermolecular interactions. Dominant hydrogen bonding interactions such as O…H (53.4%) control the molecular orientations resulting is facile charge transfer. High first-order molecular hyperpolarizability associated with high charge transfer clearly reveals the molecular level nonlinearity.

## Acknowledgements

The authors thank the Council of Scientific and Industrial Research (CSIR), New Delhi, for financial support through research grant No. 21 (1024)/16/EMR-II, and S.S is grateful to CSIR project for the award of SRF.

## REFERENCES

[1] Manimekalai, A., Saradhadevi, N., & Thiruvalluvar, A. (2010). Spectrochim Acta., Part A, 77, 687–695.

[2] Meenatchi, V., Muthu, K., Rajasekar, M., Bhagavannarayana, G., & Meenakshisundaram, SP. (2014). Optik, 125, 4181–4185.

[3] Meenatchi, V., & Meenakshisundaram, SP. (2015). RSC Adv, 5, 64180–64191.

[4] Pal, T., Kar, T., Bocelli, G., & Rigi, L. (2003). Cryst. Growth Des, 3, 13–16.

[5] Nernst,W. Z. (1909). Physik. Chem, 67, 470.

[6] Buckley, H.E. (1951). John Wiley and sons, Inc. New York.

[7] Laudice, R.A. (1970). Prentice Hall, Inc. NewYork.

[8] Pamplin,B. R. (1980). Pergamon Press, Oxford.

[9] Hong-lan Cai, Bing Liu and Qing-an Qiao, (2014). Acta Cryst, E70, o15.

[10] Xiao-Gang Mu., Xuan- Jun Wang., Youzhi Zhang., Xiaoli Gou., & Xia Li. (2011). Acta Cryst, E67, o3378.

[11] Frisch, M. J., & Trucks, G.W. (2009). Gaussian 09, Revision C.01, Gaussian, Inc., Wallingford, CT.

[12] Dennington, R., Keith, T., & Millam, J. (2009). Gauss View, Version 5, Semichem Inc., Shawnee Mission KS.

[13] Schlegel, B. (1982). J. Comput. Chem, 3214-3218.

[14] Werner Kaminsky. (2005). J. Appl. Cryst, 38, 566–567.

[15] Macrae, C. F., Bruno, I. J., Chisholm, J. A., Edgington, P. R., McCabe, P., Pidcock, E., Rodriguez- Monge, L., Taylor, R., van de Streek, J., & Woods P. A. (2008). J. Appl. Crystallogr, 41, 466-470.

[16] Schroder, D. K. (2006). John Wiley & Sons.

[17] Da Silva, M. A., Carvalho, F. M., Cella, I. C. S., Bordallo, N.,& Sosman, H. N., (2013). Opt. Mate, 35, 543-546.

[18] Jauhar, RO. MU., & Murugakoothan, P. (2017). AIP Conf. Proc, 1832, 100005.

[19] Spackman M. A., & Jayatilaka, D. (2009). CrystEngComm, 11, 19–32.

[20] Hirshfeld, F. L. (1977). Theor. Chim. Acta, 44, 129–138.

[21] Wolff, S. K., Grimwood, D. J., McKinnon, J. J., Turner, M. J., Jayatilaka, D., & Spackman, M. A. (2012). CrystalExplorer (Version3.1), University of Western Australia.

**Appendix A. Fig. S1** Crystal packing showing π-π interactions for FHM

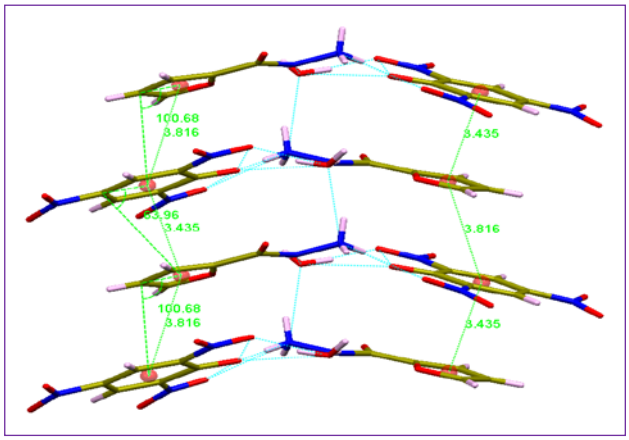


**Fig. S1.** Crystal packing showing π-π interactions for FHM

**Appendix B. Fig. S2** The structural details of N-H····O interactions

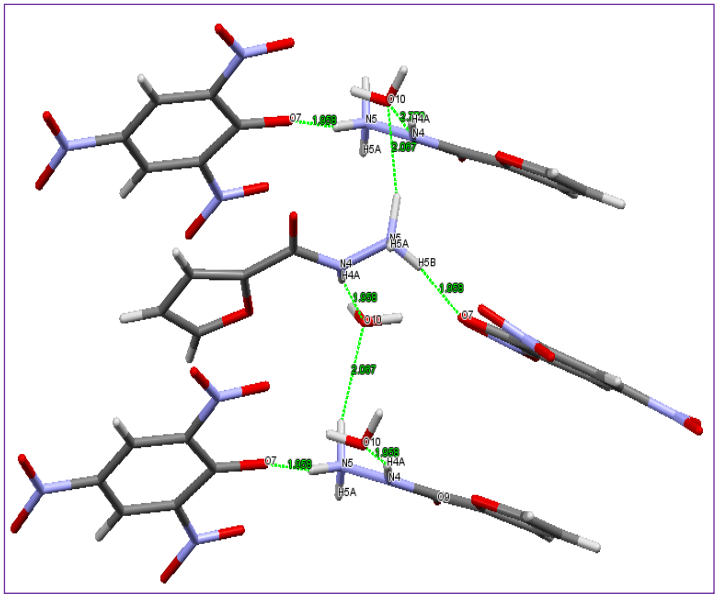

**Fig. S2** The structural details of N-H····O interactions

**Fig. S3** The structural details of C-H····O interactions

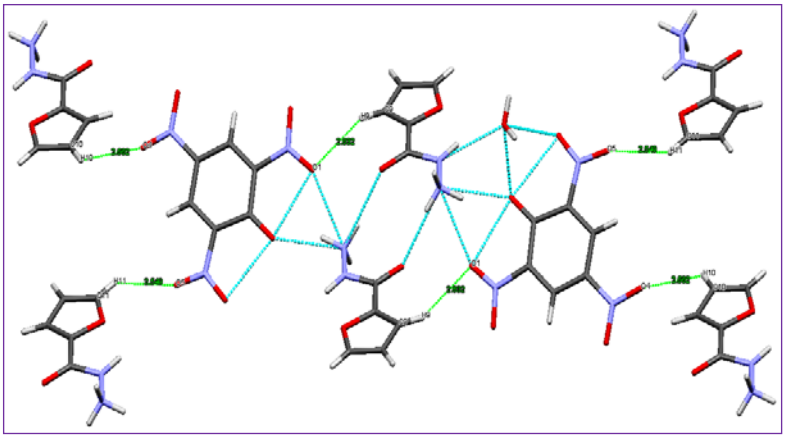

**Fig. S3** The structural details of C-H····O interactions

**Appendix C. Fig. S4** Crystal packing showing interactions along ‘a’ axis

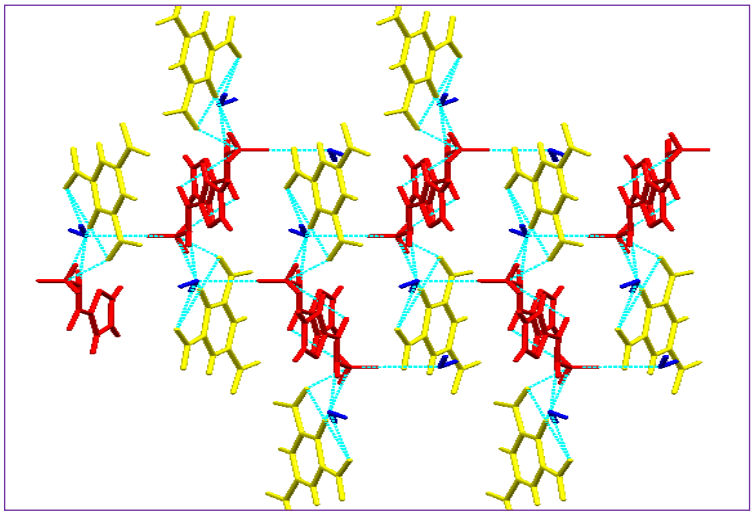

**Fig. S4** Crystal packing showing interactions along ‘a’ axis

**Appendix D. Fig. S5** Crystal packing showing interactions along ‘b’ axis

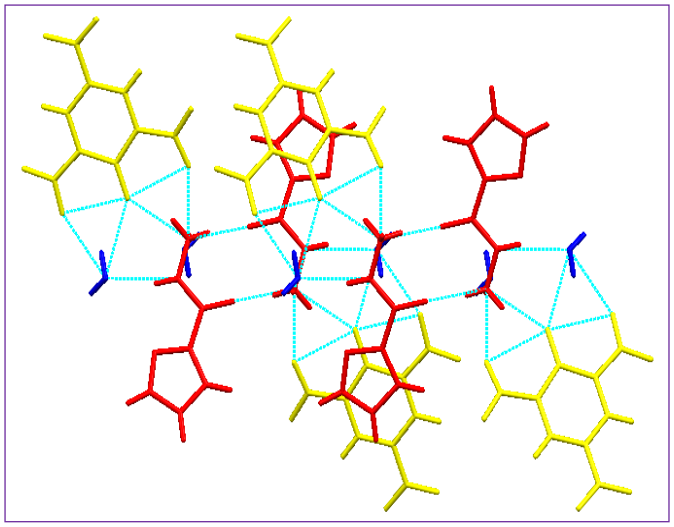

**Fig. S5** Crystal packing showing interactions along ‘b’ axis

**Appendix E. Fig. S6** Crystal packing showing interactions along ‘c’ axis

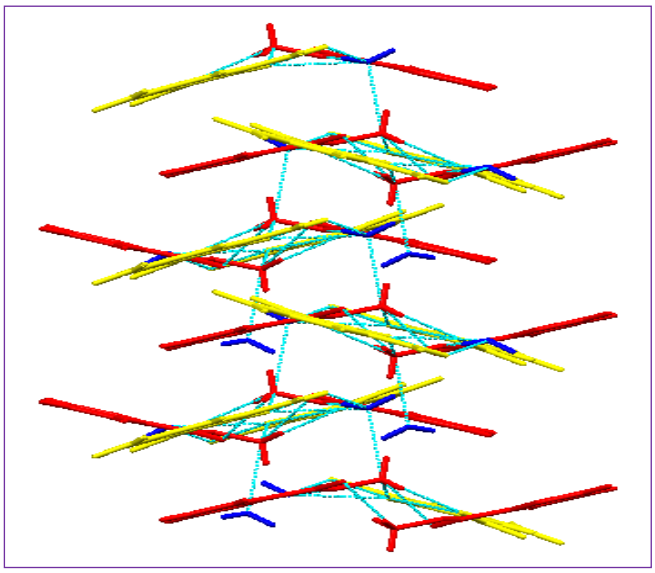

**Fig. S6** Crystal packing showing interactions along ‘c’ axis